Journal of Histochemistry & Cytochemistry 2016, Vol. 64(3) 179–189
© 2016 The Histochemical Society
Reprints and permissions:
sagepub.com/journalsPermissions.nav
DOI: 10.1369/0022155415626499
jhc.sagepub.com
SAGE

Sclerostin Immunoreactivity Increases in Cortical Bone Osteocytes and Decreases in Articular Cartilage Chondrocytes in Aging Mice

Michelle L. Thompson, Juan Miguel Jimenez-Andrade, and Patrick W. Mantyh
Department of Pharmacology, University of Arizona, Tucson, Arizona (MLT, JMJA, PWM); Unidad Académica Multidisciplinaria Reynosa Aztlan, Universidad Autónoma de Tamaulipas, Reynosa, Tamaulipas, Mexico (JMJA); and Cancer Center, University of Arizona, Tucson, Arizona (PWM).

Summary
Sclerostin is a 24-kDa secreted glycoprotein that has been identified as a negative modulator of new bone formation and may play a major role in age-related decline in skeletal function. Although serum levels of sclerostin markedly increase with age, relatively little is known about whether cells in the skeleton change their expression of sclerostin with aging. Using immunohistochemistry and confocal microscopy, we explored sclerostin immunoreactivity (sclerostin-IR) in the femurs of 4-, 9-, and 24-month-old adult C3H/HeJ male mice. In the femur, the only two cell types that expressed detectable levels of sclerostin-IR were bone osteocytes and articular cartilage chondrocytes. At three different sites along the diaphysis of the femur, only a subset of osteocytes expressed sclerostin-IR and the percentage of osteocytes that expressed sclerostin-IR increased from approximately 36% to 48% in 4- vs. 24-month-old mice. In marked contrast, in the same femurs, there were ~40% fewer hypertrophic chondrocytes of articular cartilage that expressed sclerostin-IR when comparing 24- vs. 4-month-old mice. Understanding the mechanism(s) that drive these divergent changes in sclerostin-IR may provide insight into understanding and treating the age-related decline of the skeleton. (J Histochem Cytochem 64:179–189, 2016)

Keywords
aged, cortical bone, joint, osteocyte subtype, hypertrophic chondrocyte, articular cartilage

Introduction

In humans, peak skeletal mass and strength is reached when an individual is 25–30 years old and then declines thereafter (Exton-Smith et al. 1969; Firooznia et al. 1984). By the time an individual reaches 60 years of age, diseases such as osteoporosis and osteoarthritis, which involve declines in the mass, strength and healing properties of bone or joint, become highly prevalent disorders. In preclinical and clinical studies, aging-related bone loss predisposes individuals to an increased risk of bone fracture (Melton, 1996; Ferguson et al. 2003; Yates et al. 2007). Thus, 50% of women and 25% of men over the age of 50 years will suffer age-related fractures over their lifetime (Rollman and Lautenbacher 2001). Age-related bone fractures usually heal slower than bone fractures in the young. As a result, age-related fractures are frequently accompanied by chronic skeletal pain, loss of functional status, and increased morbidity/mortality (Gruber et al. 2006).

Currently, there are two main classes of drugs available to treat age-related bone loss. The first class is the anti-resorptives (e.g., bisphosphonates, Denosumab), which work to slow bone loss by inhibiting the activity of osteoclasts. However, as bone turnover is disrupted, microcracks can

Received for publication July 13, 2015; accepted December 7, 2015.

Supplementary material for this article is available on the *Journal of Histochemistry & Cytochemistry* Web site at http://jhc.sagepub.com/supplemental.

Corresponding Author:
Patrick W. Mantyh, Department of Pharmacology, 1501 N. Campbell Ave, P.O. Box 245050, Tucson, AZ 85724, USA.
Email: pmantyh@email.arizona.edu

accumulate, compromising the integrity of bone (Chapurlat and Delmas 2009; Allen and Burr 2011). While the progress in anti-resorptive therapies has been remarkable, with long term use, the efficacy declines (Allen and Burr 2011).

The second other relevant class of drugs for treating bone loss is osteo-anabolic agents – true bone-building therapies. The first osteo-anabolic to be put into clinical use was intermittent parathyroid hormone (PTH), which exerts its effects by preferentially stimulating osteoblasts over osteoclasts (Greenfield 2012). However, bone density seems to plateau after 18–24 months of PTH therapy, and the treatment has been shown to increase the risk of osteosarcoma in rats (Vahle et al. 2002). Recombinant bone morphogenic proteins represent another anabolic option, though they are limited by their high cost and difficulty of administration (Lane and Silverman 2010). Thus, the niche for a safe and effective osteo-anabolic drug to prevent and/or treat age-related bone loss remains largely unfilled.

Recently, significant progress has been made in identifying several novel osteo-anabolic therapeutic targets (Palaniswamy et al. 2010; Lim and Clarke 2012; Ohlsson 2013). Here, we focus on one of these which is the protein sclerostin, a small (24 kDa) secreted glycoprotein that is expressed in the adult skeleton osteocytes and chondrocytes. Sclerostin acts by inhibiting the Wnt/β-catenin signaling pathway (Brunkow et al. 2001). Induction of the Wnt signaling pathway promotes bone formation whereas inactivation of the pathway leads to osteopenic states (Holmen et al. 2005). Human data suggest that there is an increase in the serum levels of sclerostin over a person's lifetime and suggest that local increases of sclerostin in bone may play an important role in age-related impairment in bone formation (Brunkow et al. 2001; Ardawi et al. 2011; Modder et al. 2011; Amrein et al. 2012; Arasu et al. 2012).

Although the great majority of research on the function of sclerostin has focused on bone, sclerostin has also been shown to be expressed in hypertrophic chondrocytes of the articular cartilage (Chan et al. 2011). Previous studies have shown that Wnt/β-catenin activity that is involved in maintaining normal cartilage and disruption of the signaling cascade can result in the development of an osteoarthritis (OA)-like phenotype. However, whether this OA phenotype is due to changes in β-catenin signaling in the subchondral bone and/or articular chondrocytes remains unclear (Yuasa et al. 2008; Zhu et al. 2008; Weng et al. 2009; Zhu et al. 2009).

In the present study, we address the largely unanswered question as to whether osteocytes and chondrocytes change their expression of sclerostin protein with age and whether they do so in concert. In order to do this, we used a specific antibody raised against sclerostin and examined the immunoreactivity in the mouse femur. The femur was chosen as it contains both osteocytes and chondrocytes. It is also a major load-bearing bone, which is a common site for age-related fractures. With age-related OA involving the articular cartilage at the head of the femur, it frequently results in the need for hip replacement.

Materials & Methods

Animals

Experiments were performed with naïve femurs obtained from young (4 months old; n=9), middle-aged (9 months old; n=3) and old (24 months old; n=4) adult male C3H/HeJ animals. The mice were housed in accordance with the National Institutes of Health guidelines under specific pathogen-free conditions in autoclaved cages maintained at 22°C with a 12-hr alternating light/dark cycle and access to food and water *ad libitum.* All procedures adhered to the guidelines of the Committee for Research and Ethical Issues of the IASP (Zimmermann 1983) and were approved by the Institutional Animal Care and Use Committee at the University of Arizona (Tucson, AZ).

Preparation of Tissues for Immunohistochemistry and Histology

At 4, 9, and 24 months of age, animals were sacrificed and perfused, as previously described (Jimenez-Andrade et al. 2008). After perfusion, the left hind limbs were removed and post-fixed for 24 hr at 4°C in the same perfusion fixative solution. The femurs were decalcified for approximately 2 weeks in 10% ethylenediaminetetracetic acid (EDTA) (PBS, pH 7.4 at 4°C; Sigma-Aldrich, St. Louis, MO). Decalcification was monitored radiographically with a Faxitron MX-20 digital cabinet X-ray system (Faxitron/Bioptics; Tucson, AZ). Following thorough decalcification, each femur was cryoprotected in 30% sucrose at 4°C for at least 48 hr to allow the sample to equilibrate and sink to the bottom of the tube before being sectioned.

Immunohistochemistry and Histology

To characterize the sclerostin-IR in young, middle-aged, and old bone, femurs were processed immunohistochemically and histologically, as previously described (Chartier et al. 2014). Immunostaining for sclerostin was performed with an antibody directed against Gln24-Tyr211 (1:400 dilution; R&D Systems, Minneapolis, MN). This polyclonal antibody detects mouse SOST/Sclerostin in direct ELISAs and western blots (Kusu et al. 2003). After overnight primary antibody incubation, preparations were washed 3 × 10 min each in PBS and incubated for 3 hr at room temperature (21°C) with secondary antibodies conjugated to fluorescent markers (Cy3; 1:600; Jackson ImmunoResearch, West Grove, PA). After a 3-hr incubation, preparations were washed 3 × 10 min each in PBS and incubated for 20 min with Alexa Fluor 488-conjugated phalloidin (Life Technologies; Grand Island, NY). Bone sections were then washed in PBS for 3 × 10 min

and counterstained with DAPI (1:500; Molecular Probes/Thermo Fisher Scientific) for 5 min. Preparations were washed again in PBS for 3 × 10 min each, and coverslipped with VectaShield (Vector Laboratories, Inc.; Burlingame, CA). Preparations were allowed to dry at room temperature for 12 hr before being imaged.

As controls for specific and non-specific sclerostin-IR staining, two methods were used: deletion of the primary antibody (data not shown) and use of a blocking peptide (R&D Systems; Minneapolis, MN). The sclerostin antibody (0.5 μg/ml) was diluted in PBS/TBS and added 5-fold (by weight) to the recombinant mouse sclerostin ("blocked"). In a separate mixture, the same dilution of antibody with the same volume of saline/PBS without the peptide ("control") was made. Both the "blocked" and "control" mixtures were allowed to incubate at room temperature for 1 hr. Following the blocking/competition incubation period, the "blocked" and "control" samples were diluted with 1%/0.1% Triton-X 100 blocking buffer and incubated on consecutive bone sections overnight at room temperature. After this primary incubation, the secondary preparation steps were carried out as described above.

Confocal images were acquired with an Olympus Fluoview FV1000 (Olympus, Center Valley, PA) system equipped with Multiline Argon (458, 488, 515 nm), Green HeNe (543 nm), Red HeNe (633 nm) lasers; and with an Olympus Fluoview FV1200 system equipped with LD (405, 440, 473, 559, 635 nm), Multiline Argon (457, 488, 515 nm), and HeNe(G) (534 nm) lasers. Each Fluoview system was equipped with multiple excitation and emission filters. Selected markers were visualized using excitation beams of 488 and 599 and emissions were detected using BA505-540 and B575-620 emission filters. DAPI was visualized using an excitation beam of 405 nm and emissions were detected using a BA430-470 emission filter. Sequential acquisition mode was used to reduce bleed-through from fluorophores. Images were obtained using Olympus UPlanApo 40×/1.30 and 60×/1.42 (FV1000) and UPlanFL N 40×/1.30 and PlanApo N 60×/1.42 (FV1200) oil objectives.

Histology

Slides of 10-μm bone sections were stained with hematoxylin and eosin for anatomical reference. Histology slides were imaged at 200× using bright-field microscopy on an Olympus BX-51 microscope equipped with an Olympus DP71 digital camera. In order to acquire an image of the whole tissue sample (femur), several images were acquired from each region then compiled in Adobe Photoshop. The images were cropped and saved as tiff files.

Quantifications

For all imaging purposes, the images for each cell type were obtained with identical acquisition exposure-time conditions. The percentage of osteocytes with detectable sclerostin-IR in the femoral cortical diaphyseal bone was quantified using immunohistochemical images obtained from young (4 months old), middle-aged (9 months old) and old (24 months old) adult femurs. The left limb from each animal was analyzed at three sites along the diaphysis: proximal diaphysis (4 mm from the top of the femoral head), mid-diaphysis (approximately 8 mm from the top of the femoral head) and distal diaphysis (3 mm from distal end of the femur). The approximate area of bone compartment that was analyzed was 280 μm (length) × 310 μm (width) × 20 μm (depth). For young animals, the sample size was n=3, 9, and 3 for the proximal diaphysis, mid-diaphysis, and distal diaphysis, respectively. For the middle-aged animals, the sample size was n=3 for all three sites. For old adult animals, the same sample size was n=4 for all three sites.

Three slides from each animal were imaged at 200x magnification. Only one of the two sections per slide was analyzed and at least 100 μm between each section was examined to prevent duplicate counting of osteocytes. The total number of osteocytes in the field of view was determined by counting the number of nuclei visible through DAPI staining and through phalloidin staining of the osteocytes. Positive DAPI nuclei forming vascular clusters were not included in the quantifications as they presumably are nuclei from endothelial cells. Then the number of sclerostin-positive osteocytes was determined by counting the number of sclerostin/DAPI/phalloidin overlays visible in each microscopic field. Finally, the total number of sclerostin-expressing cells was divided by the total number of cells to determine the percentage of osteocytes expressing sclerostin. The percentages of sclerostin-positive osteocytes were averaged among the three slides examined per animal.

To measure detectable sclerostin-IR changes of hypertrophic chondrocytes, two methods were used: sclerostin-IR cell number and relative sclerostin-IR fluorescence. To quantify the number of sclerostin-IR hypertrophic chondrocytes, three confocal images per young (4 months old, n=5) and old (24 months old, n=3) adult animals at 600x magnification were obtained. Using ImageJ (NIH; Bethesda, MD), the area of hypertrophic chondrocytes (using DAPI/sclerostin overlay as reference) was acquired for each section. Cells that were large (cell diameter of ≥8 μm), round and where sclerostin-IR had completely filled the cytoplasm were counted. Any cells with a diameter less than 8 μm was considered atrophic and dismissed in the quantification. For each image, the total number of sclerostin-IR cells was divided by the hypertrophic chondrocyte area and is presented as cells per mm^2. The number of sclerostin-IR chondrocytes was averaged among the three slides examined per animal.

To measure the relative sclerostin-IR fluorescence of the hypertrophic chondrocytes, the same area used to quantify the number of sclerostin-IR chondrocytes was used to

Table 1. Cells and areas of the mouse femur where sclerostin-IR was present in the femurs of 4, 9, and 24 month old mice.

	Sclerostin Immunoreactivity		
	Young Adult	Middle-Aged Adult	Old Adult
Cell Type	4-month-old	9-month-old	24-month-old
Osteocyte	+	++	+ + +
Osteoclast	–	–	–
Osteoblast	–	–	–
Hypertrophic Chondrocytes			
Growth plate	–	–	–
Articular cartilage	***	N.A.	*
Bone Marrow	–	–	–
Periosteum	*	**	***
Macrophage/Monocyte	–	–	–

There was a significant increase in the proportion of sclerostin-positive osteocytes with age and a significant decline in sclerostin-IR in the hypertrophic chondrocytes with age. Sclerostin-IR was not detected in osteoclasts, osteoblasts, cells within the growth plate, bone marrow, or in macrophages/monocytes. + Percentage of sclerostin-positive osteocytes: +, 30%; ++, 40%; +++, 50%. *, **, *** Graduated sclerostin-immunoreactivity; - Lack of immunoreactivity. N.A., not analyzed due to poor tissue quality of the proximal epiphysis of middle aged adult.

measure integrated optical density using Image Pro Plus v 6.0 image analysis software (Media Cybernetics, Bethesda, MD). The data are represented as relative fluorescence (arbitrary units). The quality of the proximal epiphysis for the middle-aged animals was poor and thus not quantified for either method.

To determine periosteal thickness, under the DAPI channel, three images per mid-diaphyseal periosteum per age group were taken at 400x magnification. The thickness (length measure) of the total periosteum was determined with Image J software (NIH) and averaged for each animal at each age group. For young, middle-aged, and old adult animals, the sample sizes were 4, 3 and 4, respectively.

Statistical Analysis

All statistical analyses were calculated in SigmaPlot software (San Jose, CA). One way-ANOVA was performed followed by a Tukey's post-hoc test comparing groups at each age. The significance level was set at $p<0.05$. In all cases, the investigator responsible for counting phalloidin-IR/DAPI and/or sclerostin-IR-positive osteocytes and chondrocytes was blinded to the age of each animal.

Results

Sclerostin Immunoreactivity (Sclerostin-IR) Is Detected in Cortical Bone Osteocytes and Articular Cartilage Hypertrophic Chondrocytes in the Mouse Femur

Using a polyclonal antibody against sclerostin, immunohistochemical staining of longitudinal sections of the naïve mouse femur illustrated that sclerostin-IR was expressed in two cell types: the osteocytes within cortical bone and hypertrophic chondrocytes of articular cartilage. Sclerostin-IR was not detected in the growth plate, osteoclasts, osteoblasts, macrophage/monocytes, or bone marrow (images not shown; Table 1).

In diaphyseal cortical bone, detectable levels of sclerostin-IR were present in osteocyte cell bodies, the dendrites/canaliculi of osteocytes, and the periosteum (Fig. 1). As a control for specific vs non-specific staining of the sclerostin-IR in both young (4 months old) and old (24 months old) adult animals, both primary antibody deletion (data not shown) and an absorption control were used on consecutive sections of bone (Fig. 2C, 2D).

A Subset of Sclerostin-Positive and -Negative Osteocytes Are Present in Mouse Cortical Bone

Phalloidin, a marker for F-actin (a component of the cytoskeleton that is expressed by osteocytes), was used to identify osteocytes and the dendrite/canaliculi network (Fig. 3A). Since osteocytes make up 90% to 95% of all adult bone cells (Bonewald 2011), DAPI was used to mark the nuclei of the bone cells present and because of the approximate 1:1 ratio of phalloidin to DAPI (Fig. 3B,D), both markers were used to co-stain with anti-sclerostin for osteocyte quantification. Interestingly, colocalization of sclerostin-IR with phalloidin-IR (and DAPI) highlighted two subtypes of osteocytes: sclerostin-positive and sclerostin-negative (Fig. 3A, 3C, and 3F). In the field of view at the mid-diaphysis (280 μm × 310 μm × 20 μm), out of 176.5 ± 11.5 osteocytes counted, only 68 ± 4.1 were sclerostin-positive (38%). Both populations of cells were in close

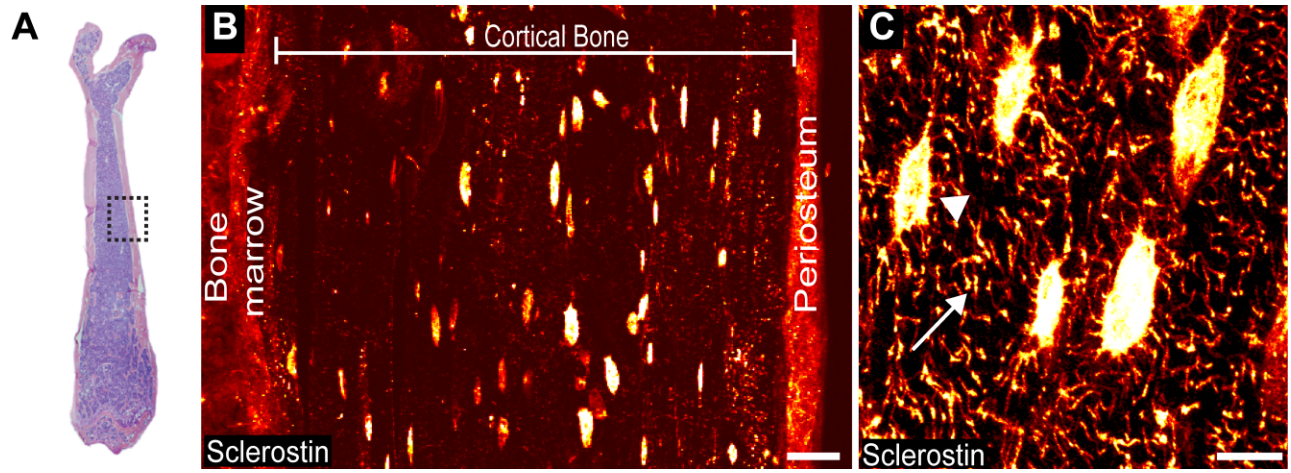

Figure 1. Detectable levels of sclerostin immunoreactivity (sclerostin-IR) are present in osteocyte cell bodies, osteocyte dendrites/canaliculi, and the periosteum in the cortical bone of the mouse femur. (A) Low power magnification, medial-lateral view of an H&E section of a young (4-month-old) male mouse femur. Boxed region indicates the mid-diaphyseal region where images in Figs. 1B, 1C, 2 and 3 were obtained. (B) Representative mid-power confocal image showing sclerostin-IR (fire red) in the osteocyte cell bodies and periosteum. (C) High-power confocal image showing sclerostin-IR within an osteocyte cell body (arrowhead) and the dendrite/canaliculi process (arrow). Scale (B) 25 μm; (C) 10 μm.

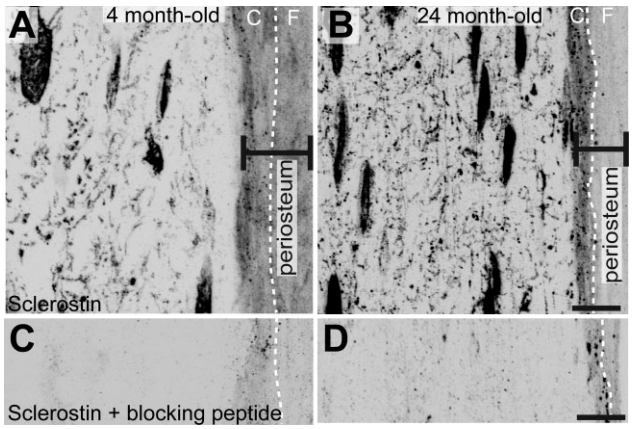

Figure 2. Sclerostin-IR in mineralized bone and adjacent periosteum (marked with black double-ended line; right), along with serially adjacent sections processed as absorption controls. (A) High-power confocal images of sclerostin-IR in mouse femoral cortical bone of young (4-month-old) and (B) old (24-month-old) adult animals. Note that sclerostin-IR is present in the osteocyte cell body, dendrite/canaliculi network, and the periosteum of young and old animals. The periosteum layers—cambium and fibrous—are demarcated by a white dashed line. (C) and (D) are serial sections of (A) and (B), respectively, and were processed the same as (A & B) except that the sclerostin antibody was replaced by a recombinant mouse SOST. Abbreviations: C, cambium layer; F, fibrous layer. Scale, 10 μm.

proximity to each other, were found throughout the width of the cortical bone (endosteal to periosteal regions), and showed similar cell body morphology. Phalloidin/DAPI/sclerostin staining also confirmed sclerostin is localized to the cytoplasm of osteocytes (Fig. 3D–3F).

The Percentage of Osteocytes That Express Detectable Levels of Sclerostin-IR Increase with Age

To determine if the subtype of sclerostin-positive osteocytes changed with age, we first examined the total number of osteocytes at the mid-diaphysis in three different age groups: young (4-month-old), middle-aged (9-month-old) and old (24-month-old) adult mice. As expected with aging, there was a decline in the total number of osteocytes. Young adult animals had an average of 176.5 ± 11.5 osteocytes; middle-aged mice had 138.7 ± 12.0 osteocytes and old adult animals had 83 ± 7.5 osteocytes per field of view (280 μm × 310 μm × 20 μm). The osteocytes that were sclerostin-positive had a slight decline with age [68.1 ± 4.1; 60.5 ± 1.7; 41.4 ± 4.0 for young middle-aged and old adults, respectively, per field of view (280 μm × 310 μm × 20 μm)]; however, the percentage (ratio) of sclerostin-positive osteocytes to total osteocytes increased with age.

At the mid-diaphysis, the percent of sclerostin-positive osteocytes increased from 38.5 ± 1.6% to 43 ± 3.6% to 49 ± 2.3% in young, middle-aged, and old adults, respectively (Fig. 4). Two additional sites along the diaphysis were also examined to determine if the increase in the number of sclerostin-positive osteocytes was dependent on location. We found that this age-dependent increase was consistent with at least a 1.3–1.4-fold change between the proximal

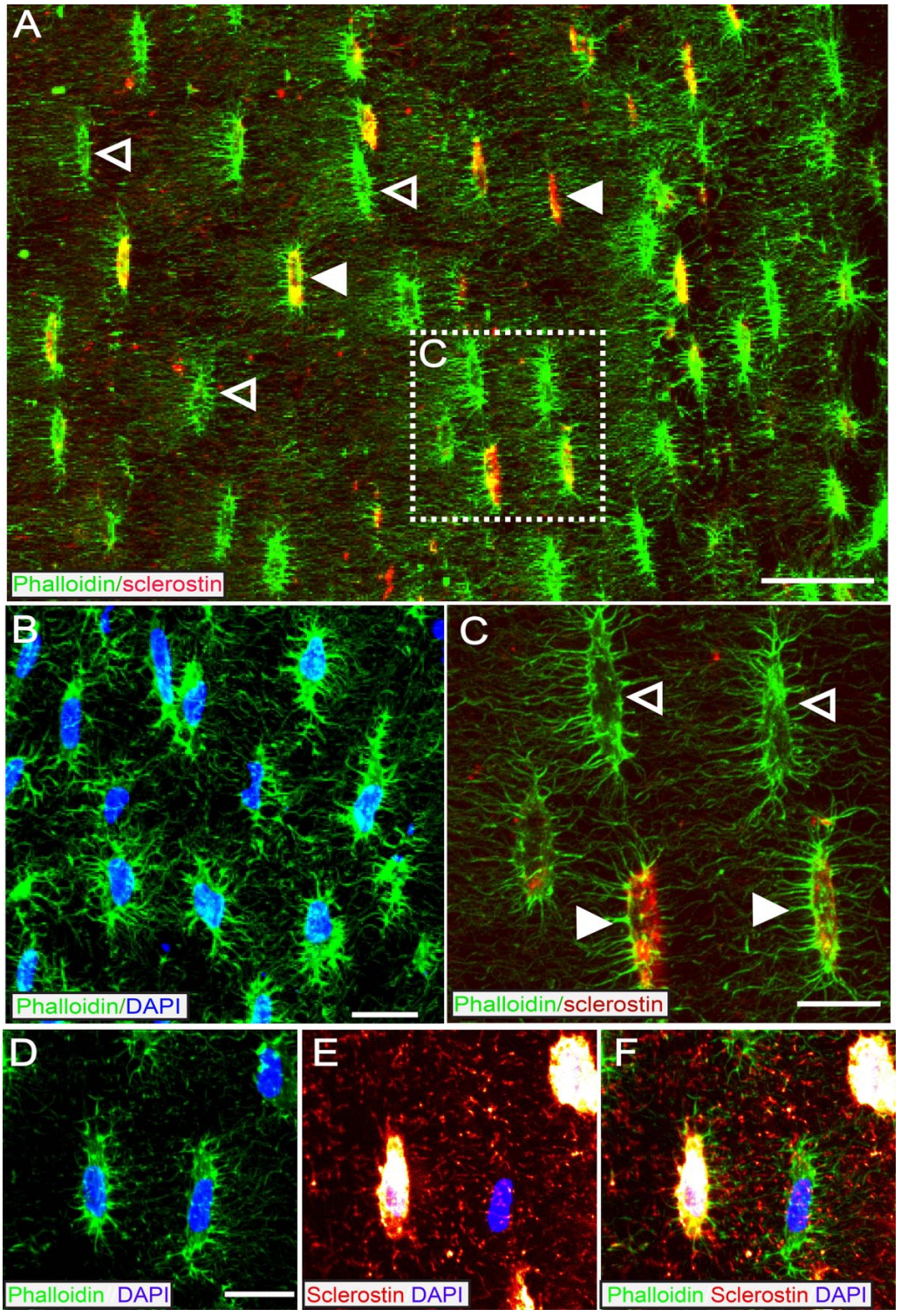

Figure 3. A subset of osteocytes that bind phalloidin (which binds to F-actin and that is expressed by osteocytes) also express detectable levels of sclerostin-IR. (A) Mid-power confocal image of cortical bone from a 4 month old animal showing co-localization of phalloidin (green) and sclerostin-IR (red). The periosteal surface is on the right and the endosteal surface is on the left. (B) High power confocal image of DAPI (blue) / phalloidin (green) overlay. Since >95% of cells in cortical bone are osteocytes there is nearly a 1:1 overlap of phalloidin and DAPI in cortical bone. (C) High power confocal image shows that the co-localization of phalloidin (green) and sclerostin (red) is only present in a subset of osteocytes (closed arrowhead). Sclerostin-negative osteocytes are demarcated by open arrowhead. (D-F) High power confocal image of phalloidin (green), DAPI (blue), and sclerostin (fire red) showing that when sclerostin-IR signal is maximized, there is clear distinction between sclerostin-IR positive and sclerostin-IR negative osteocytes. Scale bar (A) 30 μm; (B) 20 μm; (C) 10 μm; (D-F) 8 μm.

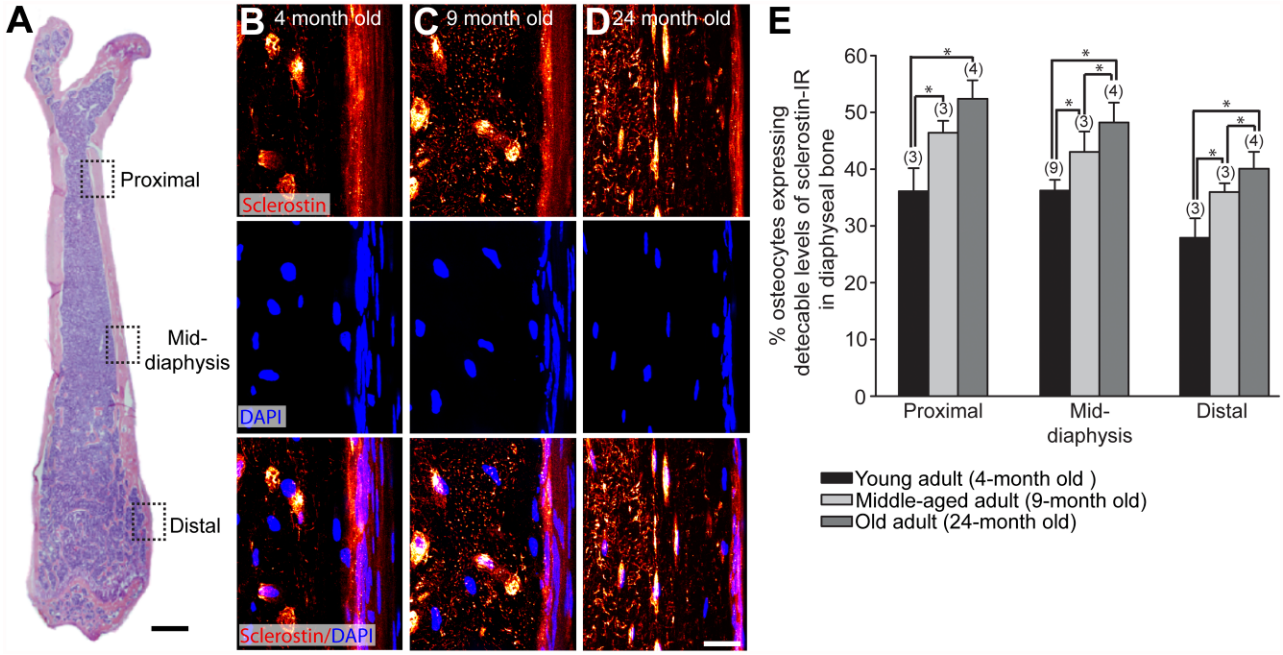

Figure 4. The percentage of osteocytes that express detectable levels of sclerostin-IR increases with age. (A) Low-power magnification, medial-lateral view H&E section of a young mouse femur showing the regions where osteocyte sclerostin-IR was analyzed in young (4-month-old), middle-aged (9-month-old), and old (24-month-old) adult C3H male mice. Three sites were selected along the diaphysis: the proximal (4 mm from the proximal head), mid-diaphysis (8 mm from the proximal head), and distal (3 mm from the distal head). (B–D) High-power confocal images of sclerostin-IR (upper panel), DAPI (middle panel) and sclerostin/DAPI overlay (lower panel) in mouse femoral cortical bone of young (B) middle-aged (C) and old (D) adult animals. (E) Histogram illustrating the percentage of osteocytes expressing detectable levels of sclerostin-IR in cortical bone in young, middle-aged, and old adult diaphyseal cortical bone. All ages were statistically significantly different from each other at each site, except middle-aged vs. old at the proximal diaphyseal region ($p>0.06$). The numbers in parentheses above each bar indicate the number of animals analyzed for each age group. Bars represent the mean ± SEM; $p<0.05$ after a one-way ANOVA, Tukey's *post-hoc* test. Scale (A) 1 mm; (B–D) 5 μm.

diaphysis, mid-diaphysis, and distal diaphysis of the young and old adult animals (Fig. 4E).

Expression of Detectable Levels of Sclerostin-IR in Articular Cartilage Hypertrophic Chondrocytes Declines with Age

In the same longitudinal sections of the femur where sclerostin-IR osteocytes were detected, sclerostin-IR was observed in the hypertrophic chondrocytes at the proximal epiphysis of the femur (Fig. 5). To determine if the age-dependent change to sclerostin-IR was conserved in this cell type, the number of hypertrophic chondrocytes per unit area with sclerostin-IR staining that completely filled the cytoplasm of the large, round hypertrophic chondrocytes with a diameter of 8 μm or greater was counted for 4-month-old (young) and 24-month-old (old) adult animals (Fig. 5G). In the old adult, a portion of the sclerostin-positive cells appeared atrophic, and these cells were not counted. In young animals, there were 286 ± 70 sclerostin-positive chondrocytes per mm^2. In the old adult, there were only 125 ± 55.7 per mm^2. Furthermore, in the same area used for cell counts, the relative sclerostin-IR fluorescence intensity measurements showed a 36% decline with age (Fig. 5F).

Discussion

There were four major findings in the present study. First, the only two cells types that expressed detectable levels of sclerostin-IR in the young, middle-aged and old mouse femurs were bone osteocytes and articular chondrocytes. Second, in the 9- and 24-month-old femurs, there was small but significant increase in the percentage of sclerostin-IR positive osteocytes as compared with that measured in 4-month-old animals. Third, sclerostin-IR was also observed in the periosteum. Lastly, the number of chondrocytes expressing sclerostin-IR declined markedly when comparing the articular cartilage of the hip joint of 24- vs. 4-month-old mice.

A Subset of Osteocytes Express Detectable levels of sclerostin in 4, 9, and 24 month old animals

Sclerostin-positive and sclerostin-negative osteocytes were often found in close proximity to one another, a surprising

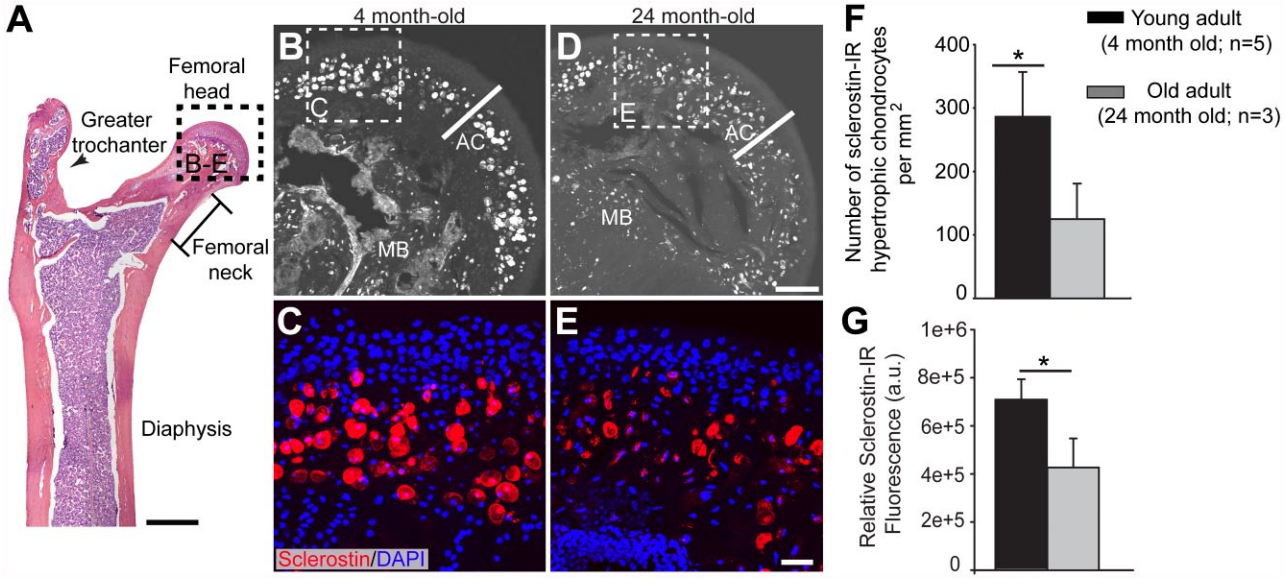

Figure 5. Sclerostin-IR in hypertrophic chondrocytes present in articular cartilage decreases in the old as compared with that in the young adult mice. (A) Representative low-power H&E section of the proximal end of the mouse femur in medial-lateral view. Boxed areas correspond to where images were obtained and analysis was performed. (B, D) Mid-power confocal image showing sclerostin-IR (white) expressed by hypertrophic chondrocytes in the articular cartilage (designated by AC) in young (4-monthold, B) and old (24-month-old, D) adult animals. (C, E) High-magnification confocal overlay of sclerostin-IR (red) and DAPI (blue) show that lower levels of sclerostin-IR and lower number of sclerostin-expressing hypertrophic chondrocytes are present in the old vs. young adult animals. (F) Histograms showing the decline in the number of sclerostin-IR hypertrophic chondrocytes in the old vs. young animals. (G) Histogram showing that the relative fluorescence of sclerostin-IR in chondrocytes declines by approximately 40% in the old vs. young animals. Bars represent mean ± SEM; $p<0.05$ after a one-way ANOVA, Tukey's *post-hoc* test. Abbreviations: AC, articular cartilage; MB, mineralized bone. Scale (A) 1 mm; (B, D) 100 μm; (C, E) 10 μm.

finding considering that immediately adjacent osteocytes would presumably be subject to similar levels of loading and mechanical stress, which have been shown to regulate the expression of sclerostin mRNA and protein in bone osteocytes (Robling et al. 2008; Moustafa et al. 2012). These subtypes of osteocytes were observed in three different sites examined in the mineralized bone of the femur, suggesting that the expression of sclerostin by a subset of osteocytes is not limited to the area of bone. Interestingly, previous studies have shown that, even in bones that received no loading for 14 days (which should increase sclerostin expression), only 50% of the osteocytes expressed detectable levels of sclerostin protein (i.e., sclerostin-IR) and mRNA (Moriishi et al. 2012). Together, these studies suggest that there is a subset of osteocytes that more readily express detectable levels of sclerostin protein and mRNA even when subjected to similar levels of mechanical loading.

The Percentage of Osteocyte Cell Bodies That Express Sclerostin-IR Increases with Age

With aging, there is loss of total bone mass so that the total number of osteocytes in the entire skeleton also decreases (Frost 1960; Dunstan et al. 1990; Halloran et al. 2002). In humans, even with the decline in the total number of osteocytes, serum levels of sclerostin (which is presumed a reflection of sclerostin that is synthesized and released by osteocytes) has been reported to increase with aging in both men and women (Mirza et al. 2010; Modder et al. 2011; Amrein et al. 2012; Bhattoa et al. 2013; Szulc et al. 2013a; Szulc et al. 2013b; Roforth et al. 2014). As increasing sclerostin levels in serum presumably arise from the ever-declining number of osteocytes, an obvious question is how do serum sclerostin levels continue to rise as the total number of osteocytes is declining?

The present study may partly address this dichotomy. First, while the total mass (and total osteocytes) of mineralized bone declines in aging mice (Almeida et al. 2007; Jilka, 2013), we show that the percentage of osteocytes that express detectable levels of sclerostin-IR increases. These data suggest that the remaining population of osteocytes may increase their protein expression and release of sclerostin, presumably allowing the ever-diminishing population of osteocytes to synthesize and release an ever-increasing amount of sclerostin in bone with aging.

Although the bone-inhibitory effects of sclerostin and molecular signaling pathway have been extensively investigated (Ke et al. 2012), its exact method of transport of sclerostin from the cell body to distant sites is less well-defined. The osteocyte dendrites are surrounded by the

canalicular wall, forming the lacuna-canalicular network (Turner et al. 2002). Between dendrites are gap junctions; yet, due to the size limitation, only proteins less than 1.2 kDa can pass through the dendrites, so it is unlikely that a molecule like sclerostin (24 kDa) will be transported between osteocyte dendrites. Even at the highest power magnification that we can achieve with confocal microscope, we cannot conclude whether the majority of sclerostin is inside or outside the dendrites or whether sclerostin-IR in the dendrites, canaliculi or periosteum increases with age. These are important questions to answer and will require further investigation with higher resolution imaging techniques.

Sclerostin-IR Is Present in the Cambium Layer of the Periosteum

Previous studies have shown that mesenchymal progenitor cells are present in the cambium layer of the periosteum and these progenitor cells play an important role in bone healing following bone fracture and bone formation in aging bone. In the present study, we showed that there is sclerostin-IR in the cambium layer of the periosteum. It is well established that the periosteum thickness declines with age in multiple species, including mouse, rat, rabbit, and human (Supplemental Fig. 1) (O'Driscoll et al. 2001; Ochareon and Herring 2007; Al-Qtaitat et al. 2010; Jimenez-Andrade et al. 2010). Notably, this decline in thickness is attributed primarily to the shrinkage of the cellular rich cambium layer, which may be why it is easier to discern sclerostin-IR in the old vs. young animals. As mesenchymal progenitor cells are known to be present in the cambium layer, it will be interesting in future studies to determine if sclerostin modulates periosteal involvement in bone formation, remodeling, and fracture repair (Guillot 2012).

The Number of Articular Cartilage Chondrocytes that Express Sclerostin-IR Declines with Age

The present results provide a unique perspective on the role of sclerostin in cartilage vs bone by simultaneously visualizing changes in the expression of sclerostin-IR in the bone and joint of the femur. Consistent with previous findings (Todd Allen et al. 2004), our data show a decrease in the number and size of chondrocytes in aging animals. Thus, in marked contrast to the increase in sclerostin-positive osteocytes found in cortical bone with aging, the number of sclerostin-IR chondrocytes declines in the 24- vs. 4-month-old animals. Interestingly, sclerostin expression by hypertrophic chondrocytes of the growth plate has previously been reported (van Bezooijen et al. 2009); although, we did not see sclerostin-IR expression in the growth plate in any of the mice examined in the present study.

Currently, a major unanswered question is: What role does sclerostin play in regulating chondrocytes and cartilage? Previous studies examining sclerostin levels in late-stage OA patients and in a sheep model of OA suggest that declining levels of sclerostin may play a role in the pathological progression of OA by inhibiting cartilage proteolysis and promoting sub-chondral bone sclerosis (Chan et al. 2011). However, in another study that utilized sclerostin-knockout mice, no obvious differences were evident in the histology of the knee joint of these animals (Roudier et al. 2013). Thus, from both a preclinical and translational perspective, developing a better understanding of the role of chondrocyte-derived sclerostin in regulating cartilage is clearly needed.

The present study demonstrates that only bone osteocytes and articular chondrocytes expressed detectable levels of sclerostin-IR in the mouse femur; that there is an increase in the percentage of sclerostin-IR positive osteocytes with aging; and that the number of chondrocytes expressing sclerostin-IR declines with age. However, there are several limitations of the present study in that only bone, one joint, one strain and one gender of mouse was used in the study. Future experiments will be needed to better understand the role sclerostin plays in the aging skeleton. These experiments will include defining whether this phenomenon occurs in females, if preferential epitope masking may also be contributing to the changes in sclerostin-IR, whether sclerostin mRNA levels in osteocytes and chondrocytes change with aging, how changes in sclerostin-IR and protein expression in osteocytes and chondrocytes correlate with changes in sclerostin-IR serum levels, and whether sclerostin regulates progenitor cells in the cambium layer of the periosteum.

Acknowledgments

The authors thank Jean-Marc Guedon, Stephane Chartier, Gwen McCaffrey, and David Sawyer for editing and reviewing the manuscript.

Author Contributions

The work described above has not been submitted for publication, in whole or in part, elsewhere, and all the authors listed have approved the manuscript that is attached. Patrick W. Mantyh (PWM) and Juan Miguel Jimenez Andrade (JMJA) and Michelle L. Thompson (MLT) conceived and designed the project. JMJA and PWM developed the methodology used. JMJA and MLT acquired the data. Analysis, interpretation of data, writing, reviewing and/or revision of the manuscript was performed by MLT, JMJA and PWM. Study supervision was led by MLT and PWM.

Competing Interests

The authors declared no potential competing interests with respect to the research, authorship, and/or publication of this article.

Funding

The authors disclosed receipt of the following financial support for the research, authorship, and/or publication of this article: This work was supported by the National Institutes of Health grants (NS23970) and National Cancer Institute grants (CA157449, CA1574550), and by the Calhoun Fund for Bone Pain.

References

Al-Qtaitat A, Shore RC, Aaron JE (2010). Structural changes in the ageing periosteum using collagen III immuno-staining and chromium labelling as indicators. J Musculoskelet Neuronal Interact 10:112-123.

Allen MR, Burr DB (2011). Bisphosphonate effects on bone turnover, microdamage, and mechanical properties: what we think we know and what we know that we don't know. Bone 49:56-65.

Almeida M, Han L, Martin-Millan M, Plotkin LI, Stewart SA, Roberson PK, Kousteni S, O'Brien CA, Bellido T, Parfitt AM, Weinstein RS, Jilka RL, Manolagas SC (2007). Skeletal involution by age-associated oxidative stress and its acceleration by loss of sex steroids. J Biol Chem 282:27285-27297.

Amrein K, Amrein S, Drexler C, Dimai HP, Dobnig H, Pfeifer K, Tomaschitz A, Pieber TR, Fahrleitner-Pammer A (2012). Sclerostin and its association with physical activity, age, gender, body composition, and bone mineral content in healthy adults. J Clin Endocrinol Metab 97:148-154.

Arasu A, Cawthon PM, Lui LY, Do TP, Arora PS, Cauley JA, Ensrud KE, Cummings SR, Study of Osteoporotic Fractures Research G (2012). Serum sclerostin and risk of hip fracture in older Caucasian women. J Clin Endocrinol Metab 97: 2027-2032.

Ardawi MS, Al-Kadi HA, Rouzi AA, Qari MH (2011). Determinants of serum sclerostin in healthy pre- and postmenopausal women. J Bone Miner Res 26:2812-2822.

Bhattoa HP, Wamwaki J, Kalina E, Foldesi R, Balogh A, Antal-Szalmas P (2013). Serum sclerostin levels in healthy men over 50 years of age. J Bone Miner Metab 31:579-584.

Bonewald LF (2011). The amazing osteocyte. J Bone Miner Res 26:229-238.

Brunkow ME, Gardner JC, Van Ness J, Paeper BW, Kovacevich BR, Proll S, Skonier JE, Zhao L, Sabo PJ, Fu Y, Alisch RS, Gillett L, Colbert T, Tacconi P, Galas D, Hamersma H, Beighton P, Mulligan J (2001). Bone dysplasia sclerosteosis results from loss of the SOST gene product, a novel cystine knot-containing protein. Am J Hum Genet 68:577-589.

Chan BY, Fuller ES, Russell AK, Smith SM, Smith MM, Jackson MT, Cake MA, Read RA, Bateman JF, Sambrook PN, Little CB (2011). Increased chondrocyte sclerostin may protect against cartilage degradation in osteoarthritis. Osteoarthritis Cartilage 19:874-885.

Chapurlat RD, Delmas PD (2009). Bone microdamage: a clinical perspective. Osteoporos Int 20:1299-1308.

Chartier SR, Thompson ML, Longo G, Fealk MN, Majuta LA, Mantyh PW (2014). Exuberant sprouting of sensory and sympathetic nerve fibers in nonhealed bone fractures and the generation and maintenance of chronic skeletal pain. PAIN 155:2323-2336.

Dunstan CR, Evans RA, Hills E, Wong SY, Higgs RJ (1990). Bone death in hip fracture in the elderly. Calcif Tissue Int 47:270-275.

Exton-Smith AN, Millard PH, Payne PR, Wheeler EF (1969). Pattern of development and loss of bone with age. Lancet 2:1154-1157.

Ferguson VL, Ayers RA, Bateman TA, Simske SJ (2003). Bone development and age-related bone loss in male C57BL/6J mice. Bone 33:387-398.

Firooznia H, Golimbu C, Rafii M, Schwartz MS, Alterman ER (1984). Quantitative computed tomography assessment of spinal trabecular bone. I. Age-related regression in normal men and women. J Comput Tomogr 8:91-97.

Frost HM (1960). In vivo osteocyte death. J Bone Joint Surg Am 42-A:138-143.

Greenfield EM (2012). Anabolic effects of intermittent PTH on osteoblasts. Curr Mol Pharmacol 5:127-134.

Gruber R, Koch H, Doll BA, Tegtmeier F, Einhorn TA, Hollinger JO (2006). Fracture healing in the elderly patient. Exp Gerontol 41:1080-1093.

Guillot D (2012). Almost invisible, often ignored: periosteum, the living lace of bone. Medicographia 34:221-227.

Halloran BP, Ferguson VL, Simske SJ, Burghardt A, Venton LL, Majumdar S (2002). Changes in bone structure and mass with advancing age in the male C57BL/6J mouse. J Bone Miner Res 17:1044-1050.

Holmen SL, Robertson SA, Zylstra CR, Williams BO (2005). Wnt-independent activation of beta-catenin mediated by a Dkk1-Fz5 fusion protein. Biochem Biophys Res Commun 328:533-539.

Jilka RL (2013). The relevance of mouse models for investigating age-related bone loss in humans. J Gerontol A Biol Sci Med Sci 68:1209-1217.

Jimenez-Andrade JM, Bloom AP, Stake JI, Mantyh WG, Taylor RN, Freeman KT, Ghilardi JR, Kuskowski MA, Mantyh PW (2010). Pathological sprouting of adult nociceptors in chronic prostate cancer-induced bone pain. J Neurosci 30:14649-14656.

Jimenez-Andrade JM, Herrera MB, Ghilardi JR, Vardanyan M, Melemedjian OK, Mantyh PW (2008). Vascularization of the dorsal root ganglia and peripheral nerve of the mouse: implications for chemical-induced peripheral sensory neuropathies. Mol Pain 4:10.

Ke HZ, Richards WG, Li X, Ominsky MS (2012). Sclerostin and Dickkopf-1 as therapeutic targets in bone diseases. Endocr Rev 33:747-783.

Kusu N, Laurikkala J, Imanishi M, Usui H, Konishi M, Miyake A, Thesleff I, Itoh N (2003). Sclerostin is a novel secreted osteoclast-derived bone morphogenetic protein antagonist with unique ligand specificity. J Biol Chem 278:24113-24117.

Lane NE, Silverman SL (2010). Anabolic therapies. Curr Osteoporos Rep 8:23-27.

Lim V, Clarke BL (2012). New therapeutic targets for osteoporosis: beyond denosumab. Maturitas 73:269-272.

Melton LJ, 3rd (1996). Epidemiology of hip fractures: implications of the exponential increase with age. Bone 18:121S-125S.

Mirza FS, Padhi ID, Raisz LG, Lorenzo JA (2010). Serum sclerostin levels negatively correlate with parathyroid hormone

levels and free estrogen index in postmenopausal women. J Clin Endocrinol Metab 95:1991-1997.

Modder UI, Hoey KA, Amin S, McCready LK, Achenbach SJ, Riggs BL, Melton LJ, 3rd, Khosla S (2011). Relation of age, gender, and bone mass to circulating sclerostin levels in women and men. J Bone Miner Res 26:373-379.

Moriishi T, Fukuyama R, Ito M, Miyazaki T, Maeno T, Kawai Y, Komori H, Komori T (2012). Osteocyte network; a negative regulatory system for bone mass augmented by the induction of Rankl in osteoblasts and Sost in osteocytes at unloading. PLoS One 7:e40143.

Moustafa A, Sugiyama T, Prasad J, Zaman G, Gross TS, Lanyon LE, Price JS (2012). Mechanical loading-related changes in osteocyte sclerostin expression in mice are more closely associated with the subsequent osteogenic response than the peak strains engendered. Osteoporos Int 23:1225-1234.

O'Driscoll SW, Saris DB, Ito Y, Fitzimmons JS (2001). The chondrogenic potential of periosteum decreases with age. J Orthop Res 19:95-103.

Ochareon P, Herring SW (2007). Growing the mandible: role of the periosteum and its cells. Anat Rec (Hoboken) 290:1366-1376.

Ohlsson C (2013). Bone metabolism in 2012: Novel osteoporosis targets. Nat Rev Endocrinol 9:72-74.

Palaniswamy C, Selvaraj DR, Rao V, Patel U (2010). Newer therapies for osteoporosis. Am J Ther 17:197-200.

Robling AG, Niziolek PJ, Baldridge LA, Condon KW, Allen MR, Alam I, Mantila SM, Gluhak-Heinrich J, Bellido TM, Harris SE, Turner CH (2008). Mechanical stimulation of bone in vivo reduces osteocyte expression of Sost/sclerostin. J Biol Chem 283:5866-5875.

Roforth MM, Fujita K, Mcgregor UI, Kirmani S, McCready LK, Peterson JM, Drake MT, Monroe DG, Khosla S (2014). Effects of age on bone mRNA levels of sclerostin and other genes relevant to bone metabolism in humans. Bone 59:1-6.

Rollman GB, Lautenbacher S (2001). Sex differences in musculoskeletal pain. Clin J Pain 17:20-24.

Roudier M, Li X, Niu QT, Pacheco E, Pretorius JK, Graham K, Yoon BR, Gong J, Warmington K, Ke HZ, Black RA, Hulme J, Babij P (2013). Sclerostin is expressed in articular cartilage but loss or inhibition does not affect cartilage remodeling during aging or following mechanical injury. Arthritis Rheum 65:721-731.

Szulc P, Bertholon C, Borel O, Marchand F, Chapurlat R (2013a). Lower fracture risk in older men with higher sclerostin concentration: a prospective analysis from the MINOS study. J Bone Miner Res 28:855-864.

Szulc P, Boutroy S, Vilayphiou N, Schoppet M, Rauner M, Chapurlat R, Hamann C, Hofbauer LC (2013b). Correlates of bone microarchitectural parameters and serum sclerostin levels in men: the STRAMBO study. J Bone Miner Res 28:1760-1770.

Todd Allen R, Robertson CM, Harwood FL, Sasho T, Williams SK, Pomerleau AC, Amiel D (2004). Characterization of mature vs aged rabbit articular cartilage: analysis of cell density, apoptosis-related gene expression and mechanisms controlling chondrocyte apoptosis. Osteoarthritis Cartilage 12:917-923.

Turner CH, Robling AG, Duncan RL, Burr DB (2002). Do bone cells behave like a neuronal network? Calcif Tissue Int 70:435-442.

Vahle JL, Sato M, Long GG, Young JK, Francis PC, Engelhardt JA, Westmore MS, Linda Y, Nold JB (2002). Skeletal changes in rats given daily subcutaneous injections of recombinant human parathyroid hormone (1-34) for 2 years and relevance to human safety. Toxicol Pathol 30:312-321.

Van Bezooijen RL, Bronckers AL, Gortzak RA, Hogendoorn PC, Van Der Wee-Pals L, Balemans W, Oostenbroek HJ, Van Hul W, Hamersma H, Dikkers FG, Hamdy NA, Papapoulos SE, Lowik CW (2009). Sclerostin in mineralized matrices and van Buchem disease. J Dent Res 88:569-574.

Weng LH, Wang CJ, Ko JY, Sun YC, Su YS, Wang FS (2009). Inflammation induction of Dickkopf-1 mediates chondrocyte apoptosis in osteoarthritic joint. Osteoarthritis Cartilage 17:933-943.

Yates LB, Karasik D, Beck TJ, Cupples LA, Kiel DP (2007). Hip structural geometry in old and old-old age: similarities and differences between men and women. Bone 41:722-732.

Yuasa T, Otani T, Koike T, Iwamoto M, Enomoto-Iwamoto M (2008). Wnt/beta-catenin signaling stimulates matrix catabolic genes and activity in articular chondrocytes: its possible role in joint degeneration. Lab Invest 88:264-274.

Zhu M, Chen M, Zuscik M, Wu Q, Wang YJ, Rosier RN, O'keefe RJ, Chen D (2008). Inhibition of beta-catenin signaling in articular chondrocytes results in articular cartilage destruction. Arthritis Rheum 58:2053-2064.

Zhu M, Tang D, Wu Q, Hao S, Chen M, Xie C, Rosier RN, O'keefe RJ, Zuscik M, Chen D (2009). Activation of beta-catenin signaling in articular chondrocytes leads to osteoarthritis-like phenotype in adult beta-catenin conditional activation mice. J Bone Miner Res 24:12-21.

Zimmermann M (1983). Ethical guidelines for investigations of experimental pain in conscious animals. PAIN 16:109-110.